Effects of thermal strain on the optical properties of heteroepitaxial ZnTe

Y. Zhang and B. J. Skromme
Department of Electrical Engineering and Center for Solid State Electronics Research, Arizona State University, Tempe, Arizona 85287-5706

F. S. Turco-Sandroff
Bellcore, Red Bank, New Jersey 07701
(Received 6 February 1992)

Optical measurements have been used to study the biaxial tensile strain in heteroepitaxial ZnTe grown by molecular-beam epitaxy on both GaAs and GaSb substrates, and its effect on the low-temperature photoluminescence (PL) spectrum of the material. The observed strain (0.92×10^{-3} for ZnTe/GaAs and 0.45×10^{-3} for ZnTe/GaSb) agrees with that expected for differential thermal contraction from the growth temperature to low temperature, based on the difference in thermal expansion coefficients. The amount of strain increases with growth temperature, as expected, but decreases slightly in thin layers on GaAs. The latter effect is due to incomplete relaxation of the large (7.6%) lattice mismatch strain between ZnTe and GaAs, the unrelieved part of which constitutes a biaxial compressive strain. Reflectance and variable temperature PL measurements show that the free exciton splits into heavy-hole (X_{hh}) and light-hole (X_{lh}) components, which both shift to lower energy. The $J=1$ (allowed) and $J=2$ (forbidden) components of the oxygen isoelectronic center bound exciton are mixed and shifted to lower energy by the strain. Temperature-dependent PL measurements show that the oscillator strengths of the two components are strongly redistributed by the strain. We calculate the strain-induced splittings in the O-bound exciton and in the excitons bound to neutral acceptors and neutral double acceptors, and find good agreement with the experimentally observed peak positions. Further confirmation of our assignments of the strain-split and shifted bound exciton peaks is obtained using magnetospectroscopy in fields up to 12 T. The diamagnetism, g factors, and splitting patterns of the free and bound excitons in the magnetic field are discussed.

I. INTRODUCTION

Due to its wide, direct band gap ($E_g=2.26$ eV at $T=300$ K), zinc telluride is of considerable interest for potential application in green light emitting devices. For the past three decades bulk ZnTe, and more recently heterostructures involving ZnTe and other II-VI materials, have been studied extensively. However, molecular-beam epitaxial (MBE) ZnTe epilayers, usually grown on III-V substrates such as GaAs and GaSb, have received relatively little attention.[1-11] The major problems in heterostructures involving II-VI epilayers on III-V substrates which are different from the case of bulk or homoepitaxial material are out diffusion of column-III and -V elements, and strain due to lattice mismatch and thermal expansion coefficient mismatch. Since there is a large lattice mismatch between ZnTe and GaAs ($\sim7.6\%$), the critical thickness for relaxation of the epilayer is very thin. Therefore the ZnTe epilayer is expected to relax completely at the growth temperature by the formation of misfit dislocations at or near the interface. These dislocations have been found to form a regular array with a spacing of about 54 Å at the interface, and are primarily of the Lomer type.[12] As the samples cool down, the process of dislocation creation will cease due to kinetic limitations. Consequently, a biaxial tensile strain in the ZnTe epilayer should be generated by the difference in the thermal expansion coefficients of ZnTe (8.3×10^{-6} K^{-1}) and GaAs (6.86×10^{-6} K^{-1}). In the case of ZnTe/GaSb, the lattice mismatch is much smaller ($\sim0.13\%$), and the thermal expansion coefficient of GaSb ($\sim7.75\times10^{-6}$ K^{-1}) is closer to that of ZnTe. The relaxation of the mismatch strain is still expected to be complete for layers of a micrometer or more thickness, so that the remaining strain should be primarily thermal, and smaller than that in ZnTe/GaAs. The ZnTe/GaSb system is in fact quite similar to the ZnSe/GaAs system, whose strain behavior has been studied extensively.[13-15]

However, the experimental situation is not yet clear. Several researchers have claimed that there is no strain in ZnTe grown on GaAs.[2-5] By comparing low-temperature photoluminescence (PL) spectra of the heteroepitaxial layers with those of bulk material, they found a one-to-one correspondence between certain peaks in each set of spectra, with no evidence of strain-induced shifts. Therefore they concluded that the epilayers are not strained and that the biaxial tensile strain due to differential thermal contraction relaxed during the cooling process. On the other hand, Dang *et al.*[6] claimed to have observed significant biaxial tensile strain in similar samples by reflectance, low-temperature PL, and optical pumping experiments. It is important to clarify this issue, since failure to recognize strain in the material will result in incorrect assignments of the peaks in the PL spectra, which in turn will result in erroneous conclusions that could mislead the effort to improve the material quality.

In this investigation, we have performed detailed

reflectance, low-temperature PL, variable temperature PL, and magnetoluminescence measurements to demonstrate that significant thermal strain exists in the ZnTe/GaAs material system, and to determine its effect on various free and bound exciton peaks in the PL spectrum. Similar measurements have also been performed for ZnTe/GaSb. The reflectance spectrum of ZnTe/GaAs clearly shows that the free exciton peak splits into heavy-hole and light-hole components, which both shift to low energy compared to its position in unstrained bulk material. These results prove the existence of strain in our samples. The temperature dependence of the PL spectra is used to distinguish between the free and bound exciton peaks, since only the free excitons survive at high temperature. We also observe that the components of the oxygen isoelectronic center bound exciton mix, split, and shift to lower energy as a result of the strain in both the ZnTe/GaAs and ZnTe/GaSb samples, but to a larger degree in the ZnTe/GaAs case. These results further confirm the existence of strain. Accounting for the strain in the undoped ZnTe/GaAs material, we calculate the behaviors of the various bound excitons that are observed and reinterpret the PL spectra. Finally, we study the behavior of the free and bound exciton peaks in magnetic fields up to 12 T. From the diamagnetism and splitting patterns of the various exciton peaks, we confirm our assignment of the PL spectra.

II. EXPERIMENT

All samples were grown in a dual chamber Riber MBE system using metallic Zn and Te sources. A solid Zn_3As_2 source was used to dope some of the samples p type.[16] Most of the undoped and As-doped ZnTe/GaAs samples that will be discussed here were grown under Te-rich conditions with a (2×1) surface reconstruction. The growth temperature was 320–330 °C, and the layer thicknesses are from 3.5 to 7.1 μm. The ZnTe/GaSb sample was grown under Zn-rich conditions with a $c(2\times2)$ surface reconstruction, a growth temperature of 330 °C, and a layer thickness of 1.3 μm. An additional series of ZnTe/GaAs samples was grown under Zn-rich conditions with a $c(2\times2)$ surface reconstruction at growth temperatures ranging from 270 to 350 °C and with layer thicknesses varying from 0.8 to 4.25 μm, to study the strain in the material as a function of layer thickness and growth temperature. The PL measurements were performed using excitation either by blue light at 2.8 and 2.88 eV from a dye laser with Stilbene 3 dye, or by UV light at 3.53 eV from an Ar^+ gas laser. A 12-T superconducting solenoid was used for the magnetospectroscopy; details of the apparatus have been given elsewhere.[17] The samples were suspended strain free in flowing superfluid or gaseous He in all cases.

III. RESULTS

A. Evidence for biaxial tensile strain in the epilayers

1. *Free and shallow bound excitons in ZnTe/GaAs*

Figure 1 shows the reflectance and low-temperature PL spectra for both undoped and As-doped ZnTe grown under Te-rich conditions on GaAs substrates. The reflectance spectrum for the As-doped sample clearly shows the intrinsic heavy-hole, X_{hh} ($|m_J|=\frac{3}{2}$) and light-hole, X_{lh} ($|m_J|=\frac{1}{2}$) free exciton transitions at 2.3798 and 2.3747 eV, respectively. (The reflectance spectrum of the undoped sample is not shown but is similar.) These structures match the positions of the X_{hh} and X_{lh} peaks in the PL spectra of both the undoped and As-doped samples, and agree with the assignments of Dang *et al.*[6] The much larger intensity of the X_{hh} structure in reflectance is qualitatively in agreement with theoretical expectations for the relative oscillator strengths of the X_{hh} and X_{lh} transitions in the quasicubic model,[18] assuming a weak exchange interaction, and further confirms our assignments.

For the undoped sample, we observe that the peak labeled A_1^{shallow} at 2.3694 eV is fairly weak. However, it dominates the whole spectrum and is assigned as A_1^{As} in the As-doped sample. The A_1^{As} peak in the doped sample has a full width at half maximum (FWHM) of 0.88 meV, which is narrower than those observed in previous studies,[2,3,5,6] demonstrating the high quality of the material. The correlation of this peak with As doping suggests that it almost certainly involves neutral shallow As acceptors. The structure at 2.3661 eV is possibly related to the A_1^{As} peak. Our assignment of the A_1^{As} peak is strongly supported by the observation of a corresponding "two-hole" replica at 2.3114 eV (not shown here), which involves the $2s_{3/2}$ final state of the acceptor. The energy separation between the $1s_{3/2}$ and $2s_{3/2}$ states is 57.5 meV, which is only slightly smaller than the value found for As in bulk material, 58.8 meV.[19] The difference of 1.3 meV is mainly due to strain, which is expected to reduce the $1s_{3/2}$ binding energy by 0.8 meV.[42] This observation confirms that A_1^{As} is indeed the neutral shallow As acceptor-bound exciton peak, which is further supported by the strength of its LO and TO phonon replicas. Therefore the A_1^{shallow}

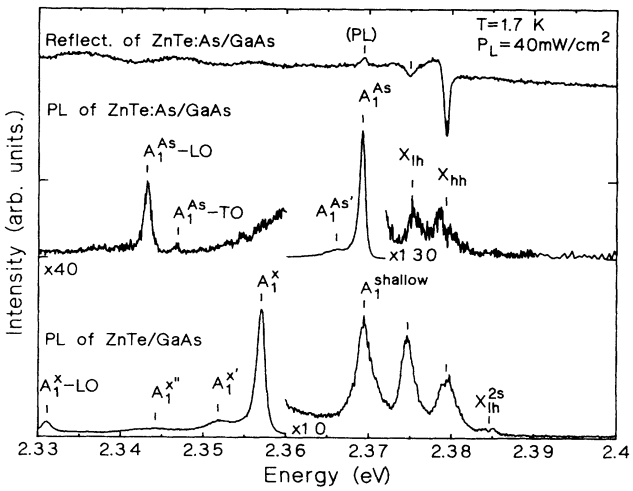

FIG. 1. Low-temperature reflectance (upper) and PL (lower two) spectra for both As-doped (7.1 μm) and undoped (3.5 μm) ZnTe/GaAs layers grown by MBE under Te-rich conditions. The small peak labeled "(PL)" in the reflectance spectrum is due to luminescence excited by the light source used for the reflectance measurement.

peak in the undoped sample, which has been shifted from its position at 2.375 eV in bulk material, is a neutral shallow acceptor-bound exciton involving acceptors such as Li, As, P, etc. These acceptors have very nearly the same A_1 peak positions in ZnTe.[19] We have not yet been able to detect the two-hole replica of A_1^{shallow} in the undoped material, which could distinguish among these possibilities. However, a $(e-A^0)$ peak involving As has been detected in this material.[10]

Our assignments of the above peaks differ strongly from those of Refs. 2, 3, and 5, where the 2.3747-eV X_{lh} peak was assigned to an (unshifted) neutral acceptor-bound exciton peak by comparison to bulk material. Our assignment of this peak to an intrinsic (rather than extrinsic) transition has obvious implications for the assessment of material quality. Also, the above authors assigned the A_1^{shallow} peak as the unshifted A_1^c peak previously observed at 2.3690 eV in bulk material,[20,21] which has been attributed to a center of orthorhombic symmetry involving donor-V_{Zn} complexes.[22] We view this match in peak positions as a purely coincidental result of the previously unrecognized strain shifts. The importance of performing careful PL measurements under a variety of conditions (as discussed below), and of correlating PL with other data such as reflectance to achieve a reliable assignment of the spectra, is made very clear in the present case.

The strongest peak in the undoped sample at 2.3570 eV is denoted A_1^x, and exhibits a corresponding LO phonon replica and two satellite peaks at 2.3518 and 2.3442 eV. A similar peak at 2.3613 eV in bulk ZnTe has been identified as an exciton bound to neutral double acceptors, which might be column-IV elements on a Te site.[23–25] Due to the strain in our material, we believe that A_1^x is that peak shifted to lower energy by strain, in agreement with the conclusions of Dang *et al.*[6] Our assignment of this peak differs significantly from that in Refs. 2 and 3, where a similar, but much broader structure was assigned as the 1LO phonon replica of an unsplit free exciton peak (it was not identified at all in Ref. 5). This reassignment is important in evaluating the properties of the undoped material grown under Te-rich conditions, which we find to be dominated by double acceptors as opposed to intrinsic transitions using the assignment of Refs. 2 and 3. These double acceptors can (hopefully) be eliminated using more highly refined source materials, which have been highly successful in improving the purity of undoped ZnSe.[26] However, the involvement of residual C from the MBE ambient is also possible, and further work will be required to distinguish these possibilities.

The excitonic features in the present material are much stronger than the donor-acceptor and band-acceptor peaks at lower energy,[10] unlike the case of solid ZnTe source-grown material of Refs. 2 and 3. Clearly, the use of high-quality elemental sources seems to produce much better purity, which is to be expected as the high-temperature synthesis of the ZnTe source material likely results in the incorporation of additional impurities from the ambient. This observation is in accord with the data of Refs. 4–6.

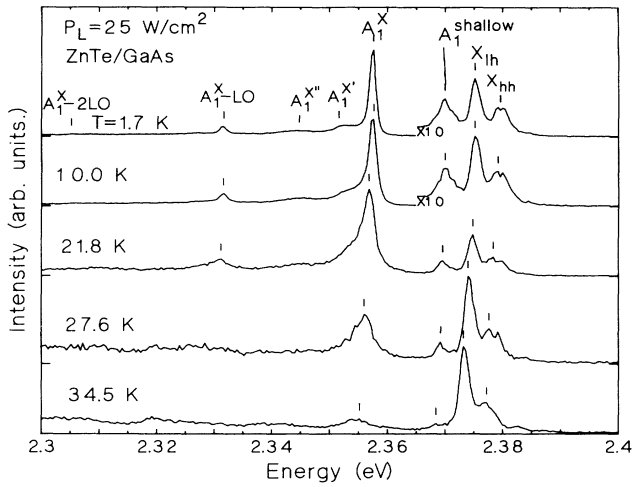

FIG. 2. Excitonic PL spectra of the undoped ZnTe/GaAs sample of Fig. 1 as a function of temperature.

Variable temperature PL spectra of the excitonic region of the undoped sample are shown in Fig. 2. The A_1^x and A_1^{shallow} peaks quench faster than the free exciton peaks. At high temperature the free excitons become the dominant features. These results further confirm that A_1^x and A_1^{shallow} are bound excitons and that X_{hh} and X_{lh} are free excitons. The small peak at 2.3846 eV in Fig. 1 is assigned to the 2*s* state of the light-hole exciton, which is confirmed below using magnetospectroscopy. The unexpectedly large strength of the X_{hh} peak relative to the X_{lh} peak in Fig. 1 is presumably due to the larger oscillator strength of the former and incomplete spin thermalization of the holes. The incomplete thermalization may be due in part to the strain splitting of the valence band. Also, the unexpectedly large strength of the 2*s* light-hole exciton is attributed to laser-induced carrier heating and incomplete thermalization. Observation of excited states such as these is not uncommon in other semiconductors under similar conditions.

The energy of the 2*s* state can be used to calculate the band gap of the material. Using the Luttinger parameters given in Ref. 28, we obtain $\mu=(6\gamma_3+4\gamma_2)/5\gamma_1=0.58$, which is the spherical effective mass parameter for the valence band in the theory of Baldereschi and Lipari.[27] Reference 27 gives the acceptor energy spectrum as a function of the parameter μ. The calculation also applies to the exciton case if μ is scaled by a factor $\alpha=\gamma_1/(\gamma_1+m_0/m_e^*)=0.34$, where we take $m_e^*=0.116m_0$.[28] Therefore $\mu'=\mu\alpha=0.20$ for the free exciton and we obtain an effective Rydberg energy $R_0=12.8$ meV from the 9.9-meV separation of the 1*s* and 2*s* X_{lh} peaks, using the results in Table III of Ref. 27. The free exciton binding energy is then given by

$$E_x=R_0\{1+\tfrac{10}{7}(\mu_0/\mu_1)^2+\tfrac{5}{28}(\mu_0/\mu_2)^2\}=13.3 \text{ meV},$$

where $1/\mu_0=1/m_e^*+\gamma_1/m_0$, $1/\mu_1=\gamma_2/m_0$, $1/\mu_2=2\sqrt{3}/m_0$. This value agrees well with $E_x=13.2\pm0.3$ meV obtained in Ref. 19 for bulk material.

The light-hole band gap in the undoped sample is reduced to about 2.3881 eV at 1.7 K by strain. All of the peaks in Fig. 2 are observed to shift to lower energy as T increases, due to the reduction in the band gap. Over the range 0–47 K, this dependence can be accurately modeled by the expression

$$E_g(T)=2.3882-1.8318\times10^{-6}\ T^2$$

where E_g is in eV and T is in K.

2. *Free and shallow bound excitons in ZnTe/GaSb*

Figure 3 shows both reflectance and PL spectra of a ZnTe/GaSb sample grown under Zn-rich conditions. A PL spectrum of a ZnTe/GaAs sample grown under the same conditions is also shown for comparison. Since the strain is relatively small in ZnTe/GaSb, due to the relatively small difference in thermal expansion coefficients ($\alpha_{ZnTe}-\alpha_{GaSb}=5.5\times10^{-7}$ versus $\alpha_{ZnTe}-\alpha_{GaAs}=1.4\times10^{-6}$), the splitting of the free exciton structure is not clearly resolved in the reflectance spectrum. However, the PL spectrum of ZnTe/GaSb shows X_{hh} and X_{lh} peaks which are split and shifted to lower energy compared to bulk material. Variable temperature PL measurements similar to those in Fig. 2 have been done to prove that the peaks at 2.3807 and 2.3785 eV are the X_{hh} and X_{lh} free excitons, respectively, and that the peak at 2.3722 eV is a bound exciton. Comparing the PL spectrum of ZnTe/GaAs in Fig. 4 with that of ZnTe/GaAs grown under Te-rich conditions in Fig. 1, we conclude that the peak at 2.3685 eV is the neutral shallow acceptor-bound exciton. Unlike the PL spectrum of Fig. 1, which shows a dominant double acceptor-bound exciton, the spectrum of the sample grown under Zn-rich conditions exhibits a strong peak at 2.3685 eV and an "undulation structure" extending to 2.345 eV. A similar undulation structure has been studied in bulk material,[33–35] and is assigned to excitons bound to closely spaced pairs of neutral acceptors. However, there is a dip between the $A_1^{shallow}$ peak and the undulation structure wing in our sample, which is not typically observed in bulk material.[33–35] This result suggests that the pairs in our material may be preferential in nature, but the details of the preferential pairing mechanism will be discussed elsewhere. Comparing the two PL spectra in Fig. 3, we find that they are very similar except for differences in the amount of shift to lower energy. Therefore we assign the peak at 2.3722 eV as the neutral shallow acceptor-bound exciton, and the structures in the range 2.3682–2.35 eV as preferential acceptor pair bound excitons in the PL spectrum of ZnTe/GaSb.

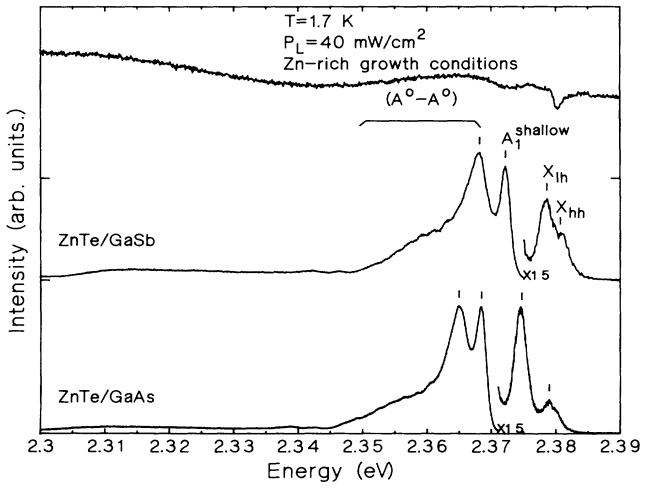

FIG. 3. Low-temperature PL (middle) and reflectance (top) spectra for a 1.3-μm-thick ZnTe layer on a GaSb substrate and a PL spectrum of a 1.6-μm-thick ZnTe layer on a GaAs substrate (bottom), all grown by MBE under Zn-rich conditions.

3. *O-bound exciton in ZnTe/GaAs and ZnTe/GaSb*

Figure 4 shows the low-energy portion of the PL data for the sample of Fig. 2 as a function of temperature. We observe two highly structured peaks X_1 at 2.1844 eV and X_2 at 2.1488 eV, which are not fully understood so far. The peaks below 2 eV are the oxygen isoelectronic center bound exciton peak and its phonon replicas. In bulk material, the $J=\frac{1}{2}$ electron, which is tightly bound to the O isoelectronic center by a short-range potential, couples via an exchange interaction to the $J=\frac{3}{2}$ hole captured by the Coulomb attraction of the electron to generate $J=1$ and 2 states. The exchange interaction splits these states, which produce peaks at 1.986 and 1.9843 eV in the PL spectrum of bulk material, respectively.[29,30] At temperatures below 4.2 K, the higher-energy $J=1$ state is thermally depopulated and only the forbidden emission from the $J=2$ state is observed in bulk material.[29] At higher temperature, $J=1$ state is thermally populated and the allowed transitions from this level produce the dominant structure in the PL spectrum, due to the much shorter lifetime resulting from the stronger oscillator strength of this state.[29] However, in our material strain has mixed and shifted the two states. New peaks are observed at 1.9816 and 1.9856 eV. The oscillator strengths are also redistributed. At around 27.6 K we observe

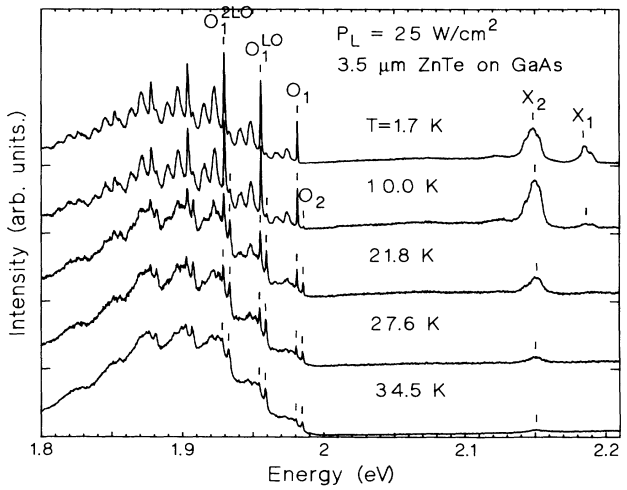

FIG. 4. Temperature dependence of the oxygen isoelectronic center bound exciton PL spectra for the sample of Fig. 2.

comparable strengths for the peaks involving transitions from the two new mixed states to the $J=0$ ground state, which is markedly different from the unstrained case. These results strongly confirm that biaxial tensile strain exists in MBE ZnTe on GaAs. Similar measurements of the O isoelectronic center bound exciton in ZnTe on GaSb have also been performed. Since the strain in ZnTe/GaSb is relatively small, the mixing and shifts of the $J=1$ and 2 states are smaller than those in ZnTe/GaAs. We observe the O_1 and O_2 peaks at 1.9828 and 1.9855 eV in the ZnTe/GaSb sample.

4. *Comparison with literature assignments*

A chart of the observed peaks and corresponding assignments for bulk material, ZnTe/GaSb, and ZnTe/GaAs reported by various authors is shown in Figs. 5(a) and 5(b). It is immediately apparent from this figure that with only a few exceptions, the same basic peaks are nearly universally observed in ZnTe grown on GaAs or GaSb, even though previous assignments have varied considerably. Superficially, several of the peaks appear to line up with certain peaks in bulk material, but this effect is merely coincidental as discussed above. The assignments given by other workers for MBE material in Refs. 2, 3, 5, and 6 have been discussed above; in the following we briefly discuss other conflicting assignments, particularly for grown by metal-organic chemical-vapor deposition (MOCVD).

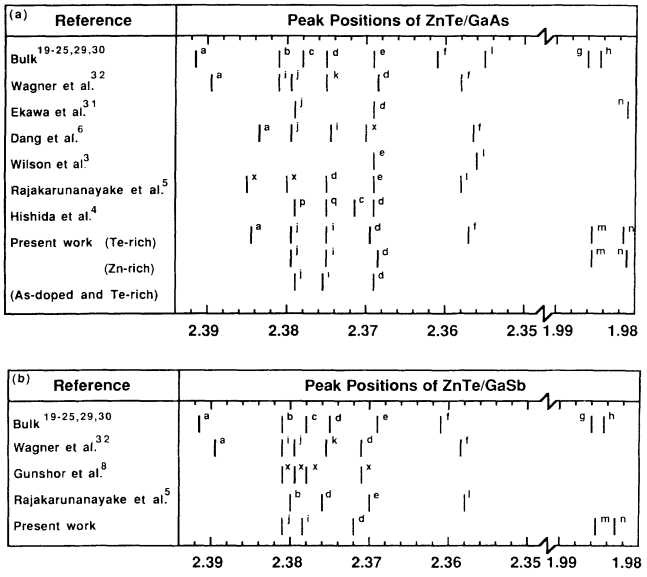

FIG. 5. (a) Observed peak positions and corresponding assignments in the PL spectra of ZnTe/GaAs by various authors. (The peak positions of Dang *et al.* have been uniformly shifted to higher energy by 1 meV in order to achieve a better alignment of their spectra with others and to correct for possible differences in calibration.) (b) As for part (a), but for ZnTe/GaSb. In both parts of the figure, $a=X_{\rm lh}^{2s}$, $b=X$, $c=(D^0,X)$, $d=A_1^{\rm shallow}$, $e=A_1^c$, $f=A_1^x$, $g=O_{J=1}$, $h=O_{J=2}$, $i=X_{\rm lh}$, $j=X_{\rm hh}$, $k=(D_{\rm Ga}^0,X)/(D_{\rm Ga}^0,h)$, $l=X_{\rm LO}$, $m=O_2$, $n=O_1$, $p=UPB$, $q=LPB$, and x is unidentified.

Based on the (O,X) peak positions and $X_{\rm hh}$ and $X_{\rm lh}$ reflectance structures, Ekawa *et al.*[31] reached similar conclusions concerning the strain and strain-induced shifts to those given here for ZnTe/GaAs grown by MOCVD. However, Wagner *et al.* have given notably different assignments for the PL spectra of ZnTe/GaAs and ZnTe/GaSb grown by MOCVD.[32] For the PL spectra of ZnTe/GaAs, the peaks at 2.3806 and 2.3795 eV are identified as $X_{\rm lh}$ and $X_{\rm hh}$, respectively, which indicates that the material is under biaxial compressive stress. However, the peaks at 2.3693 and 2.3580 eV are assigned to the shallow As acceptor-bound exciton and double acceptor-bound exciton, respectively. Compared with the positions of the same peaks in bulk material at 2.3750 and 2.3613 eV, we find that the two peaks are shifted to lower energy, which indicates that the material is under biaxial tensile strain. This inconsistency indicates that the assignments are incorrect. The peak at 2.3742 eV was assigned to a Ga donor to valence-band transition $(D_{\rm Ga}^0,h)$, partly due to its increased intensity in Ga-doped ZnTe/GaAs. The variable temperature PL spectra of Ref. 32 show that the structures at 2.38 eV and the $(D_{\rm Ga}^0,h)$ peak become the dominant features at high temperature. Such behavior might be consistent with either assignment [$X_{\rm lh}/X_{\rm hh}$ or $X_{\rm hh}/(D^0,h)$]. However, in view of our very clear reflectance spectra and the clear evidence of biaxial tensile strain in the (O,X) peaks, we assign these two peaks as $X_{\rm lh}$ and $X_{\rm hh}$ in agreement with Ekawa *et al.*[31] The splitting of the $X_{\rm hh}$ peak in the PL spectra of Wagner, Kuhn, and Gebhardt[32] might be due to polariton effects. The peak at 2.3894 eV was assigned to be a 2s state of $X_{\rm hh}$ in Ref. 32. The separation of the 2s state and $X_{\rm hh}$ ground state is 9.9 meV, which agrees with the separation of the 1s and 2s states of $X_{\rm lh}$ in the PL spectra of Dang *et al.*[6] and in the present work. Since the free exciton binding energy is mainly determined by the electron mass, which implies that the $X_{\rm hh}$ and $X_{\rm lh}$ excitons have negligibly different binding energies, we concur with the assignment of the peak at 2.3894 eV to the $X_{\rm hh}$ 2s exciton.

Hishida *et al.* gave a very different assignment to the PL spectra of ZnTe/GaAs, in which the peaks at 2.3787 and 2.3747 eV were associated with the upper and lower polariton branches associated with an unsplit free exciton.[4] However, the peak positions given by various workers are all more or less aligned with those in the present work, which indicates that all MOCVD and MBE heteroepitaxial samples are essentially similar and the strain effect has to be accounted for in deducing the correct assignments.

The same comments also apply to the PL spectra of ZnTe/GaSb. Since the strain in ZnTe/GaSb is smaller than that in ZnTe/GaAs, the PL spectra show a smaller splitting and shift to lower energy. However, the relatively small strain was not recognized in Ref. 32 in ZnTe/GaSb, and the peak at 2.3712 eV in ZnTe/GaSb that we believe is the same $A_1^{\rm shallow}$ peak as in ZnTe/GaAs was assigned to a new $(A_{\rm Sb}^0,X)$ peak. PL spectra of ZnTe on GaAs with GaSb buffer layers have been shown in Rajakarunanayake *et al.*[5] and Phillips

et al.[9] Unlike the spectra of ZnTe/GaSb, the spectra of ZnTe/GaSb/GaAs are similar to that of ZnTe/GaAs, since the ZnTe layer still suffers the strain generated from the different contraction between ZnTe and the GaAs substrate. A quantitative analysis of the PL spectra in the strained material and further confirmations of our assignments are given in the following section.

B. Quantitative analysis of the PL spectra of strained ZnTe

1. Free exciton

The free exciton in bulk ZnTe occurs at 2.3810 eV.[19] The shift and splitting of this peak in Figs. 1 and 3 indicate that a biaxial tensile strain exists in both ZnTe/GaAs and ZnTe/GaSb. In order to quantify this strain, we calculate the splitting and shift of the free exciton. Neglecting the weak exchange interaction and any effects due to the longitudinal/transverse splitting, the shifts of X_{lh} and X_{hh} for a biaxial tensile stress p in the (001) plane are given by

$$\Delta E_{lh} = \phi - \varepsilon$$

and

$$\Delta E_{hh} = \phi + \varepsilon ,$$

where $\phi = 2a(S_{11}+2S_{12})p$, $\varepsilon = -b(S_{11}-S_{12})p$, a and b are the hydrostatic and shear deformation potentials of the exciton, respectively, S_{11} and S_{12} are the compliance coefficients, and p is taken to be positive for a tensile stress. Using $a = -5.48$ eV and $b = -1.30$ eV, and the compliance coefficients given in Ref. 36, we calculate the strain and stress to be $\sim 0.92\times10^{-3}$ and ~ 0.61 kbar in the undoped ZnTe on GaAs sample and $\sim 0.45\times10^{-3}$ and ~ 0.30 kbar in the ZnTe/GaSb sample. These values are based on the experimentally measured 5.1- and 2.5-meV splittings between the X_{lh} and X_{hh} peaks in ZnTe/GaAs and ZnTe/GaSb, respectively. The temperature-dependent thermal expansion coefficients of ZnTe, GaAs, and GaSb given in Ref. 37 have been used to calculate the expected thermal strains in our heterostructures. By integrating those coefficients with respect to temperature from 1.7 K to the growth temperature, we obtain expected thermal strains of $\sim 1.1\times10^{-3}$ and $\sim 0.5\times10^{-3}$ for ZnTe/GaAs and ZnTe/GaSb, respectively. These results agree well with the values of $\sim 0.92\times10^{-3}$ and $\sim 0.45\times10^{-3}$ calculated above from the experimental data, and indicate that the source of the biaxial tensile strain in the epilayers is due to differential contraction. A series of samples of ZnTe on GaAs grown with different growth temperatures and layer thicknesses has been measured to confirm this conclusion.

The positions of the X_{hh} and X_{lh} peaks as a function of growth temperature are shown in Fig. 6. From these data, we observe that the X_{hh} and X_{lh} peaks shift to lower energy and that the separation of the X_{hh} and X_{lh} peaks increases with growth temperature. These data show that the strain increases with growth temperature and agree well with the theoretical calculation described below (represented by the solid lines in the figure), which supports our assertion that the strain in the epilayer is

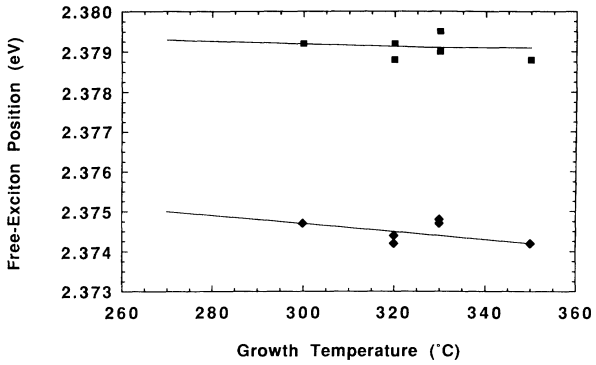

FIG. 6. Peak positions of X_{hh} (squares) and X_{lh} (diamonds) for ZnTe on GaAs as function of growth temperature with layer thickness in the range from 1.6 to 2.2 μm. The points are the experimental data and the solid lines are the theoretical calculation described in the text.

generated by the different thermal contraction of the two materials. The theoretically expected thermal strain in the epilayers as a function of growth temperature is calculated by integrating the thermal expansion coefficients of ZnTe and GaAs in Ref. 37. This calculation is based on the splitting and positions of the X_{hh} and X_{lh} peaks of the sample grown at 300 °C, which we assume to be due entirely to thermal strain.

In Fig. 7, we see that the X_{hh} and X_{lh} peaks shift to lower energy, and the separation of the X_{hh} and X_{lh} peaks increases with layer thickness for samples grown in a narrow range of temperature. This observation clearly indicates that the tensile strain in the ZnTe layer increases with layer thickness. Since the outer regions of the thicker layers are further from the interface and the biaxial compressive strain associated with the lattice mismatch is more fully relaxed, they will suffer larger net thermal strain. Furthermore, the linewidth of the X_{lh} peak becomes narrower in thicker layers, due to the smaller inhomogeneous strain resulting from defects near the interface. Similar results have been obtained for

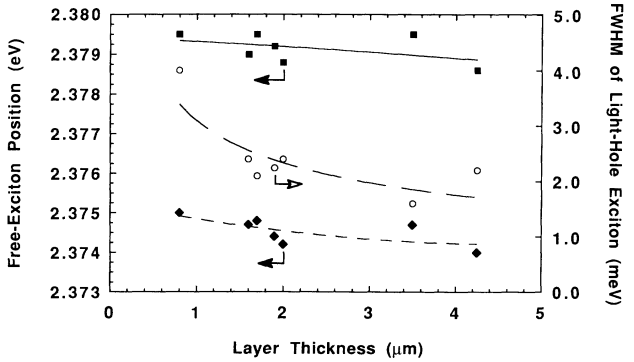

FIG. 7. Peak positions of X_{hh} and X_{lh} and FWHM of the X_{lh} peak (circles) for ZnTe on GaAs as a function of layer thickness with growth temperature in the range 320–330 °C. The squares and diamonds correspond to the X_{hh} and X_{lh} peaks, respectively. The lines are merely to guide the eye.

ZnSe/GaAs.[38] These observations suggest that some residual lattice mismatch strain probably exists in the samples of Fig. 6, but should be roughly constant since the layer thickness is about constant. However, it cannot be completely ruled out that more efficient relaxation of the compressive lattice mismatch stress at higher growth temperature may account for part of the trend observed in Fig. 6.

2. *Neutral double acceptor-bound exciton* A_1^x

In order to verify our assignment of the A_1^x peak, we compare the experimental peak position to the shift expected for the strain value determined above. In bulk material, the A_1^x peak occurs at 2.3613 eV with two broad structures 2 and 5 meV to lower energy, as reported by Magnea *et al.*[23] Dean *et al.*[25] modeled the A_1^x peak and its related structures, and studied the splitting patterns of this peak in magnetic and uniaxial stress fields. Using the model of Dean *et al.*,[25] we calculate the behavior of the A_1^x peak in a biaxial tensile strain field. Since A_1^x shows a strong diamagnetic shift rate of 6.7×10^{-3} meV T^{-2} in our sample, which is characteristic of a hydrogenic state having an effective mass of $m_e^*=0.108m_0$ comparable to the free electron mass of $0.116m_0$ in ZnTe,[28] we conclude that the electron in the A_1^x complex is loosely bound and the exchange interaction between the electron and the more tightly bound holes can be ignored. (The diamagnetic shift rate is similar to that observed for this peak in bulk material, 8.7×10^{-3} meV T^{-2}.[25]) The three $J=\frac{3}{2}$ holes in the bound exciton complex couple to produce states with $J_{\rm tot}=\frac{1}{2}$, $\frac{3}{2}$, $\frac{5}{2}$, $\frac{7}{2}$, and $\frac{9}{2}$, but the Pauli exclusion principle allows only the $J_{\rm tot}=\frac{3}{2}$ state since the holes are equivalent.[39] This (spherical) state is unsplit by the cubic crystal field and transforms like the Γ_8 representation of the T_d point group. The splitting of this fourfold degenerate state under a biaxial strain is found (in the self-consistent-field approximation) by adding the strain dependencies of each of the three holes in the complex to that of the electron. The energies of the split initial states are thus given by[25]

$$E_{\pm1/2}=\phi_{\rm initial}^{DAX}+\varepsilon^{DAX}$$

and

$$E_{\pm3/2}=\phi_{\rm initial}^{DAX}-\varepsilon^{DAX}\ ,$$

where $\phi_{\rm initial}^{DAX}=2(3a_h+a_e)(S_{11}+2S_{12})p$ and $\varepsilon^{DAX}=-b^{DAX}(S_{11}-S_{12})p$, a_h and a_e are the hydrostatic shift coefficients of the holes and electron, respectively, b^{DAX} is the shear deformation potential of holes in the double acceptor-bound exciton, and the subscripts on the energies indicate the corresponding *total* values of m_{jh}. Since loosely bound complexes are derived from states near the Γ point, the hydrostatic shift coefficients of both holes and electrons should have the same values for double acceptor-bound excitons as for free and neutral acceptor-bound excitons.

The final state (after recombination of the electron with one of the three holes) has two remaining equivalent holes which couple to generate $J=0$, 1, 2, and 3 states, but only the $J=0$ and 2 states are allowed by the Pauli exclusion principle.[39] The $J=2$ state is further split by the cubic crystal field into two states in unstrained material,[40] which transform according to the Γ_3 and Γ_5 irreducible representations of T_d. The strain reduces the point symmetry group to D_{2d}, so that the state transforming as Γ_3 in T_d splits into two new states transforming as the Γ_1 and Γ_3 representations of D_{2d}, as determined from the compatibility tables of Ref. 40. The $\Gamma_5(T_d)$ state becomes $\Gamma_4+\Gamma_5$ in D_{2d}, but these states remain degenerate in the self-consistent-field approximation for a [100] strain. The ground state of the neutral double acceptor is assigned as having T_d (Γ_3) symmetry by Dean *et al.*,[25] based on its observed splitting under a [100] stress. The Hamiltonian $H_{\gamma,\beta}$ representing the shear-strain matrix, which includes the hole-hole exchange interaction and the crystal-field splitting of the two-hole $J=2$ state, has been given and diagonalized for the case of *uniaxial* strain, e.g., by Mathieu, Camassel, and Ben Chekroun.[41] The result is the same for biaxial stress if the hydrostatic term is appropriately modified. By setting the strain term in $H_{\gamma,\beta}$ equal to zero, we obtain the energy levels of the Γ_1, Γ_3, and Γ_5 states, which are generated from the two-hole exchange interaction and the crystal-field splitting (see below for $p=0$). From the PL data for unstrained bulk material[23] and the expressions for these three levels, Dean *et al.* obtained the two-hole interaction coefficient γ and the cubic field splitting coefficient β as -0.9 and -4.8 meV, respectively[25] (apparently our definition requires the opposite sign for β to that in the convention used by Dean *et al.*).

The energies of the final two-hole states in a biaxial tensile stress p in the (001) plane are given by

$$E_i=E_0+\phi_{\rm final}^{DAX}+\Delta E_i\ ,$$

where ΔE_i ($i=1$–4) are the eigenvalues of the $H_{\gamma,\beta}$ perturbation Hamiltonian, $\phi_{\rm final}^{DAX}=4a_h(S_{11}+2S_{12})p$, and E_0 is the energy of the neutral acceptor level at zero stress. Diagonalizing $H_{\gamma,\beta}$ then yields

$$E_1=E_0+\phi_{\rm final}^{DAX}+\tfrac{1}{4}\gamma-\tfrac{2}{5}\beta,\quad T_d(\Gamma_5)\rightarrow D_{2d}(\Gamma_{4,5})\ ,$$

$$E_2=E_0+\phi_{\rm final}^{DAX}+\tfrac{3}{4}\gamma+\tfrac{3}{10}\beta+[\tfrac{1}{4}(\gamma-\tfrac{3}{5}\beta)^2+4(\varepsilon^{DAX})^2]^{1/2}\ ,\quad T_d(\Gamma_1)\rightarrow D_{2d}(\Gamma_1)\ ,$$

$$E_3=E_0+\phi_{\rm final}^{DAX}+\tfrac{1}{4}\gamma+\tfrac{3}{5}\beta,\quad T_d(\Gamma_3)\rightarrow D_{2d}(\Gamma_3)\ ,$$

and

$$E_4=E_0+\phi_{\rm final}^{DAX}+\tfrac{3}{4}\gamma+\tfrac{3}{10}\beta-[\tfrac{1}{4}(\gamma-\tfrac{3}{5}\beta)^2+4(\varepsilon^{DAX})^2]^{1/2}\ ,\quad T_d(\Gamma_3)\rightarrow D_{2d}(\Gamma_1)\ ,$$

where the corresponding representations for each state in both T_d and D_{2d} are indicated. We assume for lack of better information that b^{DAX} is the same for both initial and final states.

Transitions involving all four final states above are allowed in our configuration (Faraday, σ-polarized light), which can be seen as follows. In the initial state, we have

three coupled equivalent holes which together transform as Γ_8 in T_d. In D_{2d} symmetry, Γ_8 becomes $\Gamma_6+\Gamma_7$, which are each twofold degenerate. Two of the holes must transform according to one of these representations in an antisymmetric manner to satisfy the Pauli principle, while the third must transform as the other representation. We therefore have (in D_{2d}) either $\{\Gamma_6\times\Gamma_6\}\times\Gamma_7=\Gamma_1\times\Gamma_7=\Gamma_7(\pm\frac{1}{2})$, or $\{\Gamma_7\times\Gamma_7\}\times\Gamma_6=\Gamma_1\times\Gamma_6=\Gamma_6(\pm\frac{3}{2})$, where $\{\ \}$ denotes the antisymmetric direct product. The electron transforms as Γ_6 in both T_d and D_{2d}, so we have $\Gamma_7\times\Gamma_6=\Gamma_3+\Gamma_4+\Gamma_5$ or $\Gamma_6\times\Gamma_6=\Gamma_1+\Gamma_2+\Gamma_5$ as the total representations of the initial state in D_{2d}. Each triplet of representations remains degenerate in the limit of zero electron-hole exchange interaction. The electric dipole operator transforms as Γ_5 (D_{2d}) for σ polarization, so that transitions from $\Gamma_i \Longleftrightarrow \Gamma_f$ are allowed only if $\Gamma_5\times\Gamma_f$ contains Γ_i. We have $\Gamma_5\times\Gamma_1=\Gamma_5$, $\Gamma_5\times\Gamma_3=\Gamma_5$, $\Gamma_5\times\Gamma_4=\Gamma_5$, and $\Gamma_5\times\Gamma_5=\Gamma_1+\Gamma_2+\Gamma_3+\Gamma_4$. All transitions from each degenerate triplet to each of the four final states Γ_1, Γ_3, Γ_1, and $\Gamma_{4,5}$ in D_{2d} are therefore σ allowed. However, the higher-energy level in the initial state is thermally depopulated, so only transitions from the lower ($\Gamma_6\times\Gamma_6$) or $|m_{jh}|=\frac{3}{2}$ energy level are observed in the low-temperature PL data. The relative oscillator strengths were calculated in Ref. 25 using the coupling coefficients as 3:1:3 for ($\Gamma_6\times\Gamma_6$) to the Γ_1, Γ_3, and $\Gamma_{4,5}$ final states in D_{2d}. Transitions involving the higher-energy final states are apparently lifetime broadened.

Using the deformation potentials $a_e+a_h=-5.4$ eV and $b^{DAX}=-0.27$ eV measured for the A_1^x peak in bulk material,[25] we calculate the peak positions involving the $|m_{jh}|=\frac{3}{2}$ initial state and final states from E_1 to E_4 for the strain in the undoped ZnTe/GaAs sample to be 2.3514, 2.3538, 2.3562, and 2.3567 eV. In Fig. 1 we observe three peaks at 2.3442, 2.3518, and 2.357 eV. The theoretically expected peaks at 2.3567 and 2.3562 eV are close to the experimental peak at 2.357 eV, but only the 2.3567-eV peak is observed since the oscillator strength of that peak is three times that of the peak at 2.3562 eV. The position of the satellite at 2.3518 eV agrees well with the theoretical value (2.3514 eV). The 2.3538-eV peak is unresolved in our spectra, presumably due to inhomogeneous strain broadening. The excellent overall agreement with the theoretical calculations strongly supports our assignment. However, this model cannot explain the lower-energy satellite at 2.3442 eV. A corresponding peak has also been observed at 2.348 eV in bulk material (see Fig. 1 in Ref. 23), but was not explained there either.

3. *Shallow neutral acceptor-bound exciton*

Since the strain in our sample shifts the position of the A_1^{shallow} peak, we conclude that the A_1^{shallow} peak is the regular shallow neutral acceptor-bound exciton. This peak occurs at 2.375 eV in bulk material.[19] A calculation for this peak in a biaxial strain field must be performed to compare with the experimental results. The initial state of a neutral single acceptor-bound exciton has two holes and an electron. Neglecting the small interaction between the electron and the holes, the energy levels of two-hole states in biaxial strain for the initial state of this complex are similar to that of the final state for the double acceptor-bound exciton, except for the hydrostatic and shear deformation terms which are now $\phi_{\text{initial}}^{NAX}=2(2a_h+a_e)(S_{11}+2S_{12})p$ and $\varepsilon^{NAX}=-b^{NAX}(S_{11}-S_{12})p$, respectively. The values of the parameters γ and β characterizing the hole-hole and crystal-field interactions may be different from the double acceptor case, due to the different charge on the acceptor core. Using perturbation theory for the shear deformation potentials of hydrogenically bound holes yields $b^{NAX}/b=1-4\mu^2/5-12\mu\delta/25$,[42] where $\mu=(6\gamma_3+4\gamma_2)/5\gamma_1$ and $\delta=(\gamma_3-\gamma_2)/\gamma_1$ and the parameters are taken from Ref. 28. Thus we obtain $b^{NAX}=-0.91$ eV, and keep a_e+a_h the same as that of the double acceptor exciton in the calculation for the reason mentioned in the preceding section. Strictly speaking this value of b^{NAX} only applies to the final state (the neutral acceptor), but we assume that is also a reasonable approximation for the holes in the bound exciton.

The PL spectra recorded at higher temperature (10 K) of both the As-doped sample of Fig. 1 and a separate 4.25-μm-thick ZnTe/GaAs sample (not shown) grown under Zn-rich conditions show a high-energy component at 2.3717 eV, which must involve a transition from a higher-energy level in the initial state. Unfortunately, very little information is available concerning the splitting of the unperturbed As acceptor-bound exciton in bulk ZnTe. The summary chart given by Venghaus and Dean[19] suggests that this exciton has two components separated by about 0.2 meV. If we assume that this result for bulk material is true, then we have two possible models. The first model considers that the cubic field splitting in the shallow neutral acceptor-bound exciton is negligible compared with the hole-hole interaction. Therefore the hole-hole interaction gives $J=0$ and 2 levels which form the initial states in zero-strained material, and the magnitude of γ is the separation of the two levels and equal to 0.2 meV from the results for bulk material. The $J=2$ level shifts and splits into two levels in a biaxial strain field, and the initial states for the neutral single acceptor become three levels. The final state is a neutral acceptor, which shifts and splits into light- and heavy-hole states in the biaxial strain field. The transitions from the initial states to the lower-energy level in the final state are assumed to be the ones that are resolved in the experiment, since transitions to the higher-energy level in the final state will suffer lifetime broadening.[25] Using this model we obtain a much larger energy separation for the resolved peaks in the strained material than what is experimentally observed. This result suggests that cubic field splitting must be present for the A_1^{shallow} peak in bulk material.

The second model follows the latter assumption. Since the cubic field splits the $J=2$ state but not the $J=0$ state, there are three levels in the initial state for bulk material, of which only two levels (separated by 0.2 meV) are apparently observed due to thermalization. The energy levels in the initial state of the shallow acceptor-bound exciton in a biaxial strain field are similar to the energy

levels (E_1, E_2, E_3, and E_4) in the final state of the double acceptor-bound exciton discussed in the preceding section. The levels E_3 and E_4 are degenerate for $\gamma-3\beta/5>0$ and the levels E_2 and E_3 are degenerate for $\gamma-3\beta/5<0$ in unstrained material, respectively. There are seven possible orderings for the energy levels of the initial state in bulk material. Three of these involve $\gamma>0$ and four involve $\gamma<0$. Using the data reported for bulk material and the data we have for ZnTe/GaAs, we can obtain consistent fits in four of the seven cases. We find that γ is 1.61 or 2.24 meV and β is -0.2 or 0.2 meV, respectively, for the cases with $\gamma>0$, and γ is -1.16 or -0.48 meV and β is 1.69 or 2.4 meV, respectively, for the cases with $\gamma<0$. From the existing, limited results for bulk material and the data for strained material we cannot clearly distinguish among the various possible models, but we are able to achieve satisfactory fits to our data with plausible values of γ and β.

The variable temperature PL spectra of the ZnTe/GaSb sample of Fig. 3 also show a barely resolved high-energy component at 2.3733 meV, which is separated from the low-energy component by 1.3 meV. Together with the strain ($\sim 0.45\times10^{-3}$) for ZnTe/GaSb we obtained in Sec. III B 1 and the values of γ and β determined above for the various models, we calculate the components in strained ZnTe/GaSb, and obtain reasonably good agreement with the experimental observation for all of the possible models we proposed above. More uniaxial and zero-stress studies on bulk material are required to identify the energy levels in the initial states and to understand better the behavior of the neutral shallow acceptor-bound exciton in a biaxial strain field.

4. *The oxygen isoelectronic center bound exciton*

The O isoelectronic center bound exciton and its phonon replicas in bulk ZnTe have been studied extensively.[29,30,43–47] Since a biaxial tensile exists in our samples, the $J=1$ and 2 states resulting from the exchange interaction between the $J=\frac{1}{2}$ electron and the $J=\frac{3}{2}$ hole will mix and shift. Therefore the oscillator strengths of the transitions involving these mixed states will be redistributed. The effective perturbation Hamiltonian for a biaxial stress p in the (001) plane for this exciton is

$$H=\Delta_1\mathbf{J}_h\cdot\sigma+\phi^{OX}+\varepsilon^{OX}\left[J_{hz}^2-\frac{J_h^2}{3}\right],$$

where $\phi^{OX}=2a^{OX}(S_{11}+2S_{12})p$ and $\varepsilon^{OX}=-b^{OX}(S_{11}-S_{12})p$, Δ_1 is the coefficient for the spherical portion of the electron-hole exchange interaction, and $\mathbf{J}_h$ and σ are the hole and electron spinors. The cubic component of the exchange interaction is neglected. Diagonalizing the Hamiltonian, we get

$$E_1=\tfrac{3}{2}\Delta_1+\phi^{OX}+\varepsilon^{OX},$$

$$E_2=\tfrac{3}{2}\Delta_1+\phi^{OX}-\varepsilon^{OX},$$

$$E_3=-\tfrac{5}{2}\Delta_1+\phi^{OX}-\varepsilon^{OX},$$

and

$$E_{4,5}=-\tfrac{1}{2}\Delta_1+\phi^{OX}\pm\{(\varepsilon^{OX})^2-2\Delta_1\varepsilon^{OX}+4\Delta_1^2\}^{1/2}.$$

Transitions from levels 1 and 2 to the $J=0$ (Γ_1) ground state are forbidden, transitions from levels 3 and 4 are π and σ allowed, respectively, and transitions from level 5 become σ allowed only at finite stress. Since the electron is tightly bound in the short-range potential of the O isoelectronic center, the hydrostatic deformation potential of the electron is related to that of the entire conduction band, rather than just the Γ point as in the loosely bound case. The hydrostatic deformation potential of the weakly bound hole should be just that of the top of the valence band. We obtain the values of the net (electron plus hole) hydrostatic parameter a^{OX} and the hole shear potential b^{OX} by fitting to the experimental points. From the peak separation between the $J=1$ and 2 states in unstrained bulk ZnTe,[29,30] Δ_1 is calculated to be -0.425 meV. By fitting the experimental points in the ZnTe/GaAs sample of Fig. 4 to the above expressions for E_4 and E_5, using the stress values deduced from the free exciton splitting, we obtain $a^{OX}=-1.92$ eV and $b^{OX}=-0.73$ eV. The b^{OX} value is close to -0.91 eV, which was calculated for a hydrogenically bound hole in Sec. III B 3. This result agrees with the model for (O,X) in which a hole is loosely bound by the Coulomb force from the electron, which in turn is trapped by its short-range interaction with O.

Figure 8 shows the experimental points and the calculated energy levels for the (O,X) peaks. We find that the data points for ZnTe/GaSb agree reasonably well with the fit based on the ZnTe/GaAs sample. The data points in the PL spectra are obtained only with σ-polarized light, since we employ backscattering from a (001) surface.

The ratio of the oscillator strength of the $J=2$ state over that of the $J=1$ state in unstrained material is approximately 0.02, due to unknown mixing mechanisms which make the transition from $J=2$ slightly allowed.[29] When strain exists in the material, these two states mix and generate two new states whose associated oscillator strengths change with the strain. The oscillator strengths of the low- and high-energy states for a free exciton have been given by Bir *et al.*[18] Since (O,X) involves a single

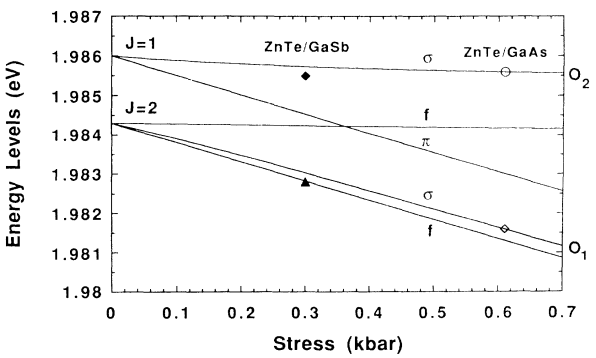

FIG. 8. Calculated energy levels of the oxygen isoelectronic center bound exciton as a function of stress (solid lines) and experimental points for ZnTe on GaSb and GaAs.

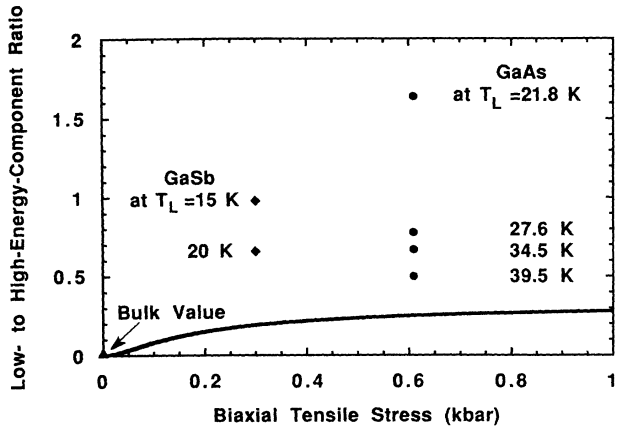

FIG. 9. Calculated oscillator strength ratio of the oxygen isoelectronic center bound exciton components as a function of stress, and data points for the corresponding peak strength ratio for ZnTe on GaSb and GaAs at various temperatures. This ratio is equal to 0.33 in the high stress limit. The point at 39.5 K for ZnTe/GaAs has a relatively large error of about ±0.13.

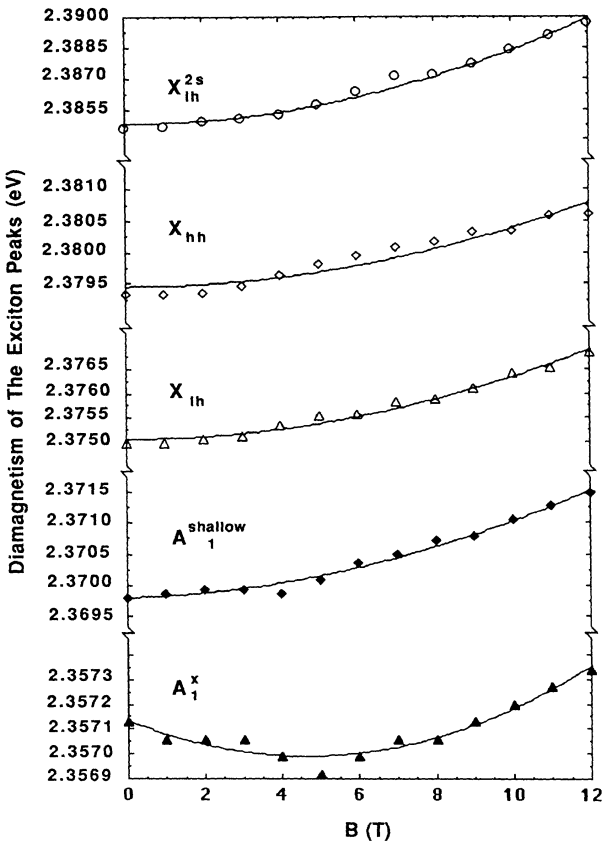

FIG. 10. Experimental data (symbols) and fitting curves (solid lines) of the diamagnetic shifts of the excitonic emissions in undoped ZnTe/GaAs. Note that each portion of the vertical axis has a different scale.

electron and hole, the situation for (O,X) is similar to that of the free exciton except for the values of the deformation potentials. In Fig. 9 we plot the distribution of the oscillator strengths as a function of stress for (O,X). The calculated value of the O_1 to O_2 peak strength ratio for the stress around 0.61 kbar in our ZnTe/GaAs sample is equal to 0.25 in the absence of thermalization. If the components are assumed to be fully thermalized, the oscillator strength ratio deduced from the observed integrated peak intensities using a Boltzmann factor would be lower than the theoretical value. In the experimental data, the peak intensity ratio at 21.8 K is 1.64. The peak intensity ratio for the 0.30-kbar stress in ZnTe/GaSb is around 0.66 at 20 K. Both values are higher than the expected values if thermalization is neglected. These results suggest that the spin components are partially but not fully thermalized at these temperatures. Additional experiments such as excitation spectroscopy or optical absorption are needed to measure the oscillator strengths accurately. However, the large increase in the ratio compared to bulk material is qualitatively in agreement with the model.

C. Magnetoluminescence

1. Diamagnetism

In addition to calculating the strain effects, we employ magnetospectroscopy to study the splitting patterns of the excitons in high magnetic fields and to check our assignments further. All magnetic field measurements were done in Faraday configuration. The diamagnetic shifts of the excitons as a function of field are shown in Fig. 10. For the 2s state of X_{lh} and the X_{hh} and X_{lh} peaks, two Zeeman split components are resolved for each peak at high fields (≥ 6 T). The average of the peak positions is therefore used when determining the diamagnetic shifts. The splitting patterns of the neutral shallow acceptor-bound exciton and the neutral double acceptor-bound exciton peaks are not well resolved. Therefore we include a linear splitting term when fitting the experimental data to determine the quadratic diamagnetic shifts. The fit curves are shown as the solid lines in Fig. 10. The diamagnetic shift of the 2s state of X_{lh} (4.2×10^{-5} eV T^{-2}) is much larger than those of the X_{lh} and X_{hh} excitons (1.3×10^{-5} and 9.4×10^{-6} eV T^{-2}, respectively). This is to be expected, since the 2s exciton has a more extended electron wave function than the 1s exciton. This observation confirms that the peak at 2.3846 eV is the 2s state of X_{lh}. The neutral shallow acceptor- and double acceptor-bound excitons have diamagnetic shifts of 1.4×10^{-5} and 6.7×10^{-6} eV T^{-2}, respectively. These results indicate that both the shallow and double acceptor-bound excitons contain loosely bound electrons, and confirm that we are justified in neglecting the interaction between the electron and the holes in these complexes.

2. Free exciton

The PL spectra of the excitons in the ZnTe/GaAs sample of Fig. 2 in both zero and high magnetic field are shown in Fig. 11. In high magnetic field, we find by comparing the σ^+- and σ^--polarized PL spectra that the X_{hh}

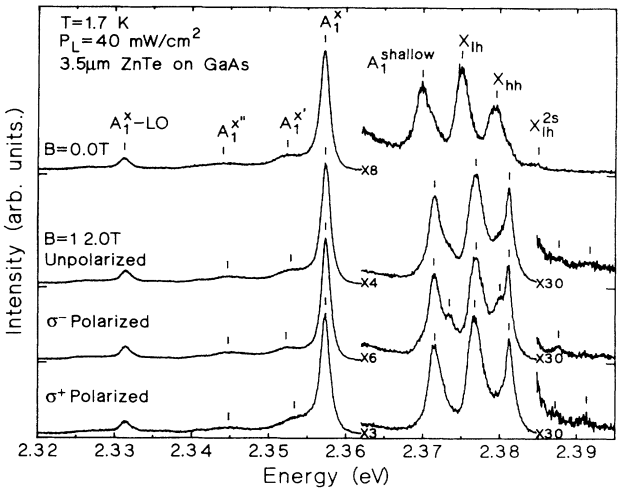

FIG. 11. Low-temperature excitonic PL spectra at $B=0$ and 12 T for the undoped ZnTe/GaAs sample of Fig. 2.

peak splits into two components while the splitting of the X_{lh} peak cannot be resolved. For a biaxial strain p along [100] and [010] and a magnetic field $\mathbf{B}$ the Hamiltonian for the free exciton is

$$H=H_{\text{Pikus}}+H_B$$
$$=\phi+\varepsilon\left[J_{hz}^2-\frac{J^2}{3}\right]+\tfrac{1}{2}g_c\mu_B\mathbf{B}\cdot\boldsymbol{\sigma}-2\tilde{\kappa}\mu_B\mathbf{B}\cdot\mathbf{J}_h$$
$$-2\tilde{q}\mu_B(J_{hx}^3B_x+J_{hy}^3B_y+J_{hz}^3B_z)$$
$$+\frac{\gamma^2}{2}R_0^*\left[c_1+\frac{c_2}{B^2}(\mathbf{J}_h\cdot\mathbf{B})^2\right],$$

where $1/\mu_0=1/m_e^*+\gamma_1/m_0$, $\gamma=e\hbar B/2\mu_0cR_0^*$, $R_0^*=\mu_0e^4/2\hbar^2\varepsilon^2$, ϕ and ε are defined in Sec. III B 1, and g_e is the electron g factor, which is related to $\tilde{g}_c=\frac{1}{2}g_e$ defined by Cho *et al.*[48] The symbols $\tilde{\kappa}$ and $\tilde{q}$ are the isotropic and cubic magnetic field splitting coefficients of the hole, respectively, μ_B is the Bohr magneton, e is the magnitude of the electron charge, c is the speed of light, m_0 is the free electron mass, and c_1 and c_2 are the diamagnetic shift coefficients. We neglect the small exchange terms, the longitudinal-transverse splitting, the anisotropic diamagnetic terms, and any second-order term involving both magnetic and strain fields. Polaron effects are also neglected, except for the use of renormalized masses. This Hamiltonian gives eight energy levels for $\mathbf{B}$ in the [001] direction. We list only those four from which σ-polarized transitions to the $J=0$ ground state are possible. For X_{hh}, we obtain

$$E_{3/2}^{\sigma^+}=-\tfrac{3}{4}\mu_BB_z(4\tilde{\kappa}+9\tilde{q})-\tfrac{1}{2}g_e\mu_BB_z$$
$$+\tfrac{1}{8}\gamma^2R_0^*(4c_1+9c_2)+\phi+\varepsilon$$

and

$$E_{-3/2}^{\sigma^-}=\tfrac{3}{4}\mu_BB_z(4\tilde{\kappa}+9\tilde{q})+\tfrac{1}{2}g_e\mu_BB_z$$
$$+\tfrac{1}{8}\gamma^2R_0^*(4c_1+9c_2)+\phi+\varepsilon\ .$$

For X_{lh}, we have

$$E_{1/2}^{\sigma^+}=-\tfrac{1}{4}\mu_BB_z(4\tilde{\kappa}+\tilde{q})+\tfrac{1}{2}g_e\mu_BB_z$$
$$+\tfrac{1}{8}\gamma^2R_0^*(4c_1+c_2)+\phi-\varepsilon$$

and

$$E_{-1/2}^{\sigma^-}=\tfrac{1}{4}\mu_BB_z(4\tilde{\kappa}+\tilde{q})-\tfrac{1}{2}g_e\mu_BB_z$$
$$+\tfrac{1}{8}\gamma^2R_0^*(4c_1+c_2)+\phi-\varepsilon\ .$$

From the peak separations of 1.19 meV between the σ^+- and σ^--polarized components of X_{hh} and approximately -0.21 meV for those of X_{lh} in Fig. 11, we obtain $g_e=-0.66$ and $\tilde{\kappa}=-0.18$ (assuming $\tilde{q}\approx0$), which are consistent with $g_e=-0.57\pm0.25$, $\tilde{\kappa}=-0.06\pm0.10$, and $\tilde{q}\approx0$ from previous magnetoreflectance measurements of the free exciton in bulk material.[49] This agreement further confirms our assignment of the light- and heavy-hole free exciton peaks. It should, however, be noted that $\gamma=0.7$ at $B=12$ T, so we are no longer in the low-field ($\gamma\leq0.4$) regime where the above perturbation theory is expected to apply. For this reason, and due to the neglect of polaron effects, we do not attempt to evaluate the actual values of c_1 and c_2.

3. *Double and neutral shallow acceptor-bound excitons*

Variable temperature PL measurements at 12.0 T (not shown) allow us to distinguish two components at 2.3572 and 2.3587 eV in σ^+-polarized spectra and one component at 2.3572 eV in σ^--polarized spectra for the neutral double acceptor-bound exciton A_1^x. The high-energy (2.3587 eV) component of the A_1^x peak appears and dominates as the temperature increases in the σ^+-polarized spectra. A broad low-energy structure associated with the A_1^x peak occurs at 2.3460 eV. The splitting of the final coupled two-hole states is believed to be unmeasurably small for $B<10$ T.[25] We still neglect this splitting for $B=12$ T. Thus the final state is the same as in zero magnetic field, which was discussed in Sec. III B 2. Using the g factors and diamagnetic shift coefficient obtained in bulk material[25] for the double acceptor-bound exciton, and keeping the other parameters the same as those in the $B=0$ case, we calculate the peak positions using the model of Dean *et al.*[25] and obtain two groups of peaks 2.3568 and 2.3571 eV (the first group), and 2.3586, 2.3588, 2.3589, 2.3591, 2.3592, and 2.3594 eV (the second group), which correspond to transitions from the lowest and second groups of energy levels in the initial states to the lowest-energy level in the final states. Given that the widths of the peaks in our PL data are limited by inhomogeneous strain broadening, we cannot distinguish these individual transitions. Transitions to excited final states will have lifetime broadening as mentioned by Dean *et al.*,[25] and we assume they are not observed experimentally. The calculated peak positions involving the ground final state agree well with the experimental results, given our limited resolution, and further verify that A_1^x is the double acceptor-bound exciton.

For the A_1^{shallow} peak, two components at 2.3713 and

2.3734 eV in the σ^--polarized PL spectra and one component at 2.3713 eV in the σ^+-polarized PL spectra are observed. The two σ^--polarized components have the same relative intensity up to about 28.4 K and thus exhibit no detectable thermalization. When the temperature increases beyond 28.4 K, the peaks quench and we cannot resolve them clearly. Since we do not have a definite model for the neutral acceptor-bound exciton in zero magnetic field, we do not attempt any detailed analysis of the splitting of the A_1^{shallow} peak in the magnetic field.

4. *Oxygen isoelectronic center bound exciton*

Finally, we examine the splitting patterns of the O isoelectronic center bound exciton in a high magnetic field. Figure 12 shows the 16-K PL data of the O isoelectronic center bound exciton in a 12-T magnetic field. The σ^+- and σ^--polarized PL spectra show four components, denoted O_a, O_b, O_c, and O_d. Correcting for the 0.22-meV shift in the band gap from 1.7 to 16 K, we find that the corresponding peak positions at $T=1.7$ K would be 1.9807, 1.9825, 1.9857, and 1.9859 eV, respectively. In order to explain this splitting pattern, we have to consider the Hamiltonian of the oxygen isoelectronic center bound exciton in a magnetic field

$$H=H_\Delta+H_{\text{Pikus}}+H_B$$
$$=\Delta_1\mathbf{J}_h\cdot\boldsymbol{\sigma}+\phi^{OX}+\varepsilon^{OX}\left[J_{hz}^2-\frac{J_h^2}{3}\right]$$
$$+\tfrac{1}{2}g_e\mu_B\mathbf{B}\cdot\boldsymbol{\sigma}-2\tilde{\kappa}\mu_B\mathbf{B}\cdot\mathbf{J}_h\ ,$$

where we neglect the diamagnetic shift. The expressions for ϕ^{OX} and ε^{OX} were given in Sec. III B 4. The anisotropic term in Ref. 50 is zero which means O_{Te} is isotropic. Diagonalizing the Hamiltonian for $\mathbf{B}\|[001]$, we get

$$E_{1,2}=\phi^{OX}+\varepsilon^{OX}+\tfrac{3}{2}\Delta_1\pm|\mu_B B_Z(-3\tilde{\kappa}+\tfrac{1}{2}g_e)|\ ,$$

$$E_{3,4}=\tfrac{1}{2}(U_1+V_1)\pm\tfrac{1}{2}\{(U_1+V_1)^2-4[U_1V_1-3\Delta_1^2]\}^{1/2}\ ,$$

$$E_{5,6}=\phi^{OX}-\varepsilon^{OX}-\tfrac{1}{2}\Delta_1\pm\{4\Delta_1^2+\mu_B^2B_Z^2(\tilde{\kappa}+\tfrac{1}{2}g_e)^2\}^{1/2}\ ,$$

and

$$E_{7,8}=\tfrac{1}{2}(U_2+V_2)\pm\tfrac{1}{2}\{(U_2+V_2)^2-4[U_2V_2-3\Delta_1^2]\}^{1/2}\ ,$$

where

$$U_1=\phi^{OX}+\varepsilon^{OX}-\tfrac{3}{2}\Delta_1-3\tilde{\kappa}\mu_BB_Z-\tfrac{1}{2}g_e\mu_BB_Z\ ,$$
$$V_1=\phi^{OX}-\varepsilon^{OX}+\tfrac{1}{2}\Delta_1-\tilde{\kappa}\mu_BB_Z+\tfrac{1}{2}g_e\mu_BB_Z\ ,$$
$$U_2=\phi^{OX}-\varepsilon^{OX}+\tfrac{1}{2}\Delta_1+\tilde{\kappa}\mu_BB_Z-\tfrac{1}{2}g_e\mu_BB_Z\ ,$$

and

$$V_2=\phi^{OX}+\varepsilon^{OX}-\tfrac{3}{2}\Delta_1+3\tilde{\kappa}\mu_BB_Z+\tfrac{1}{2}g_e\mu_BB_Z\ .$$

Figure 13 shows the calculated curves and the experimental data points. The zero-field peak positions in the magnetoluminescence data of Fig. 13 are slightly different from those obtained in the zero-field data of Fig. 4, which were recorded at a different time. Therefore we adjust a, b, g_e, and $\tilde{\kappa}$ to fit the present data. We get a good fit for $a=-1.92$ eV, $b=-0.78$, $g_e=1.8$, and $\tilde{\kappa}=-0.37$, as shown in Fig. 13. The small change in b is ascribed to experimental error. These g factors agree excellently with the values $g_e=1.9$ and $\tilde{\kappa}=-0.34$ obtained in unstrained bulk material.[50] The energy levels corresponding to the plotted curves have been indicated in Fig. 13. In the low-field limit (prior to any anticrossings), it is easily found that transitions from levels E_1 and E_2 are forbidden, those from E_3 and E_4 are σ^+ polarized, those from E_5 are π polarized and undetectable in our (backscattering) configuration, those from E_6 are forbidden, and those from E_7 and E_8 are σ^- polarized. In these determinations we use the fact that $\mathbf{B}$ is parallel to the stress axis and does not mix the states appreciably until anticrossings occur. At each anticrossing, the states exchange their oscillator strengths, as we have verified by extrapolating clear to the high-field limit. Thus transi-

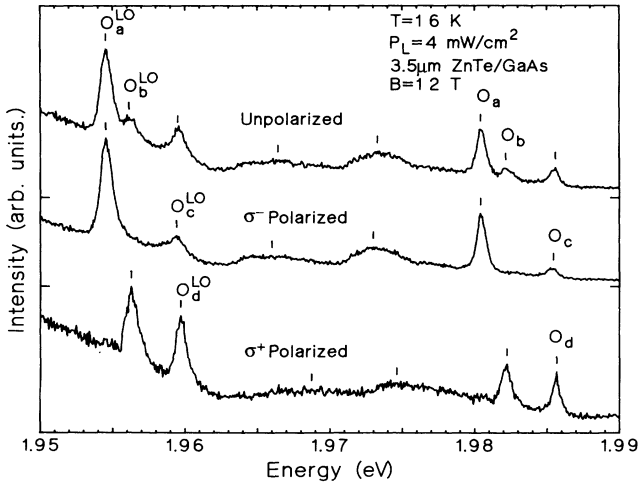

FIG. 12. Unpolarized and polarized PL spectra of the oxygen isoelectronic center bound exciton in the undoped ZnTe/GaAs sample of Fig. 2 at $T=16$ K and $B=12$ T.

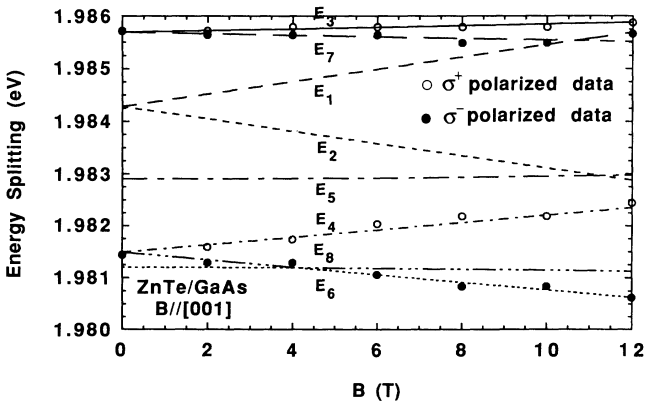

FIG. 13. Calculated energy level splitting patterns of the oxygen isoelectronic center bound exciton in a 12-T magnetic field (lines), and experimental data points for the undoped ZnTe/GaAs sample of Fig. 2.

tions from E_6 become σ^- allowed and those from E_8 become forbidden above 4.2 T, which is borne out in our fit. All data points with σ^+ and σ^- polarizations have been indicated in Fig. 13, and agree with what we expect. Similar data fits were also obtained (using the same parameters) for $\mathbf{B}\|[110]$ and $\mathbf{B}\|[111]$ (data not shown). All these good agreements verify our assignments and confirm our identification of the O-bound exciton.

IV. SUMMARY

Reflectance and variable temperature PL measurements have been performed to identify the free and bound exciton peaks in MBE ZnTe on GaAs and ZnTe on GaSb. We find that the free exciton peak splits into X_{hh} and X_{lh} components, which shift to lower energy compared to bulk material. This result shows that biaxial tensile strain resulting from the difference of the thermal expansion coefficients between ZnTe and GaAs does exist in both the ZnTe/GaAs and ZnTe/GaSb material systems. A similar shift and splitting of the two components of the oxygen isoelectronic bound exciton peak, and the redistribution of oscillator strengths of these two components from the mixing of the allowed ($J=1$) and forbidden ($J=2$) components of that peak have been observed in variable temperature PL spectra. This observation strongly supports the conclusion. From the separation of the X_{lh} and X_{hh} peaks, we calculate that the thermal strains in ZnTe/GaAs and ZnTe/GaSb samples are 0.92×10^{-3} and 0.45×10^{-3}, respectively. The strain effects as function of layer thickness and growth temperature have been studied, and show that the strain in the layer results from the differential thermal contraction of the epilayer and substrate. Failure to recognize the effects of the strain on the PL spectrum of the material will lead to incorrect conclusions about the material.

Theoretical calculations of the strain splittings and magnetospectroscopy measurements are used to further confirm our assignment of the PL spectra. In the ZnTe/GaAs sample, we calculate the strain-induced shifts and splittings of the neutral single and double acceptor-bound exciton and O-bound exciton peaks, and find that the calculated results are consistent with the experimental results. The magnitude of the diamagnetic shift is employed to confirm the identification of the $2s$ state of X_{lh}. The magnetic field splitting patterns of the free exciton, O-bound exciton, and double acceptor-bound exciton are all found to be in good agreement with theoretical calculations for strained ZnTe/GaAs. These results demonstrate that the models are reasonably valid and also verify our assignment of the excitonic emissions.

ACKNOWLEDGMENT

The ASU portion of this work was supported by the National Science Foundation under Grant No. DMR-91-06359.

[1]T. Yao, S. Amano, Y. Makita, and S. Maekawa, Jpn. J. Appl. Phys. **15**, 1001 (1976).

[2]R. D. Feldman, R. F. Austin, P. M. Bridenbaugh, A. M. Johnson, W. M. Simpson, B A. Wilson, and C E. Bonner, J. Appl. Phys. **64**, 1191 (1988).

[3]B. A. Wilson, C. E. Bonner, R. D. Feldman, R. F. Austin, D. W. Kisker, I. J. Krajewski, and P. M. Bridenbaugh, J. Appl. Phys. **64**, 3210 (1988).

[4]Y. Hishida, H. Ishii, T. Toda, and T. Niina, J. Cryst. Growth **95**, 517 (1989).

[5]Y. Rajakarunanayake, B. H. Cole, J. O. McCaldin, D. H. Chow, J. R. Soderstrom, T. C. McGill, and C. M. Jones, Appl. Phys. Lett. **55**, 1217 (1989).

[6]Le Si Dang, J. Cibert, Y. Gobil, K. Saminadayar, and S. Tatarenko, Appl. Phys. Lett. **55**, 235 (1989).

[7]D. L. Mathine, S. M. Durbin, R. L. Gunshor, M. Kobayashi, D. R. Menke, Z. Pei, J. Gonsalves, N. Otsuka, Q. Fu, M. Hagerott, and A. V. Nurmikko, Appl. Phys. Lett. **55**, 268 (1989).

[8]R. L. Gunshor, A. V. Nurmikko, L. A. Kolodziejski, M. Kobayashi, and N. Otsuka, J. Cryst. Growth **101**, 14 (1990).

[9]M. C. Phillips, Y. Rajakarunanayake, J. O. McCaldin, D. H. Chow, D. A. Collins, and T. C. McGill, *Growth of Semiconductor Structures and High-T_c Thin Films on Semiconductors* [Proc. SPIE **1285**, 152 (1990)].

[10]Y. Zhang, B. J. Skromme, and F. S. Turco, in *Electronic, Optical, and Device Properties of Layered Structures,* edited by J. Hayes, M. S. Hybertsen, and E. R. Weber, MRS Symposia Proceedings (Materials Research Society, Pittsburgh, 1990), Vol. EA-21, pp. 133–136.

[11]Y. Zhang, B. J. Skromme, and F. S. Turco-Sandroff, in *Heteroepitaxy of Dissimilar Materials,* edited by J. P. Harbison, A. Zangwill, R. Farrow, and P. S. Peercy, MRS Symposia Proceedings (Materials Research Society, Pittsburgh, 1991), Vol. 221, pp. 235–241.

[12]J. Petruzzello, D. J. Olego, X. Chu, and J. P Faurie, J. Appl. Phys. **63**, 1783 (1988).

[13]T. Yao, Y. Okada, S. Matsui, K. Ishida, and I. Fujimoto, J Cryst. Growth **81**, 518 (1987).

[14]B. J. Skromme, M. C. Tamargo, J. L. de Miguel, and R. E. Nahory, in *Epitaxy of Semiconductor Layered Structures,* edited by R. T. Tung, L. R. Dawson, and R. L. Gunshor, MRS Symposia Proceedings (Materials Research Society, Pittsburgh, 1988), Vol. 102, p. 577.

[15]B. J. Skromme, M. C. Tamargo, F. S. Turco, S. M. Shibli, W. A. Bonner, and R. E. Nahory, in *Gallium Arsenide and Related Compounds, Atlanta, 1988,* edited by J. S. Harris, IOP Conf. Proc. No. 96 (Institute of Physics and Physical Society, Bristol, 1989), p. 205.

[16]F. S. Turco-Sandroff, M. J. S. P. Brasil, R. E. Nahory, R. J. Martin, Y. Zhang, and B. J. Skromme, Appl. Phys. Lett. **59**, 688 (1991).

[17]B. J. Skromme, R. Bhat, H. M. Cox, and E. Colas, IEEE J. Quantum Electron. **25**, 1035 (1989).

[18]G. L. Bir, G. E. Pikus, L. G. Suslina, and D. L. Fedorov, Fiz. Tverd. Tela (Leningrad) **12**, 1187 (1970) [Sov. Phys. Solid State **12**, 926 (1970)].

[19]H. Venghaus and P. J. Dean, Phys. Rev. B **21**, 1596 (1980).

[20]J. L. Dessus, Le Si Dang, A. Nahmani, and R. Romestain, Solid State Commun. **37**, 689 (1981).
[21]Le Si Dang, A. Nahmani, and R. Romestain, Solid State Commun. **46**, 743 (1983).
[22]J. Bittebierre and R. T. Cox, Phys. Rev. B **34**, 2360 (1986).
[23]N. Magnea, J. L. Pautrat, Le Si Dang, R. Romestain, and P. J. Dean, Solid State Commun. **47**, 703 (1983).
[24]P. J. Dean, M. J. Kane, M. S. Skolnick, F. De Maigret, Le Si Dang, A. Nahmani, R. Romestain, and N. Magnea, J. Lumin. **31&32**, 391 (1984).
[25]P. J. Dean, M. J. Kane, N. Magnea, F De Maigret, Le Si Dang, A. Nahmani, R. Romestain, and M. S. Skolnick, J. Phys. C **18**, 6185 (1985).
[26]K. Yoneda, Y. Hishida, T. Toda, H. Ishii, and T. Niina, Appl. Phys. Lett. **45**, 1300 (1984).
[27]A. Baldereschi and N. O. Lipari, Phys. Rev. B **8**, 2697 (1973).
[28]H. Venghaus, B. Jusserand, and G. Behnke, Solid State Commun. **33**, 371 (1980).
[29]D. E. Dietz, D. G. Thomas, and J. J. Hopfield, Phys. Rev. Lett. **8**, 391 (1962).
[30]J. L. Merz, Phys. Rev. **176**, 961 (1968).
[31]M. Ekawa, Y. Kawakami, T. Taguchi, and A. Hiraki, J. Cryst. Growth **93**, 667 (1988).
[32]H. P. Wagner, W. Kuhn, and W. Gebhardt, J. Cryst. Growth **101**, 199 (1990).
[33]P. J. Dean and A. M. White, Solid State Electron. **21**, 1351 (1978).
[34]E. Molva and N. Magnea, Phys. Status Solidi B **102**, 475 (1980).
[35]N. Magnea, E. Molva, D. Bensahel, and R. Romestain, Phys. Rev. B **22**, 2983 (1980).
[36]W. Wardzynski, W. Giriat, H. Szymczak, and R. Kowalczyk, Phys. Status Solidi B **49**, 71 (1972).
[37]*Numerical Data and Functional Relationships in Science and Technology,* edited by K.-H. Hellwege, Landolt-Börnstein, New Series, Vol. 17, Parts a and b (Springer-Verlag, Berlin, 1982).
[38]See, for example, B. J. Skromme, M. C. Tamargo, J. L. de Miguel, and R. E. Nahory, Appl. Phys. Lett. **53**, 2217 (1988), and references therein.
[39]E. U. Condon and G. H. Shortley, *The Theory of Atomic Spectra* (Cambridge University Press, Cambridge, England, 1977), Table 2^{10}.
[40]G. F. Koster, J. O. Dimmock, R. G. Wheeler, and H. Statz, *Properties of the Thirty-Two Point Groups* (MIT Press, Cambridge, MA, 1963), Tables 84 and 86.
[41]H. Mathieu, J. Camassel, and F. Ben Chekroun, Phys. Rev. B **29**, 3438 (1984).
[42]M. Schmidt, Phys. Status Solidi B **79**, 533 (1977).
[43]J. J. Hopfield, D. G. Thomas, and R. T. Lynch, Phys. Rev. Lett. **17**, 312 (1966).
[44]J. D. Cuthbert and D. G. Thomas, Phys. Rev. **154**, 763 (1967).
[45]Seishi Iida, J. Phys. Soc. Jpn. **32**, 142 (1972).
[46]B. Katircioglu and J. L. Pautrat, Solid State Commun. **21**, 503 (1977).
[47]E. D. Jones, H. P. Hjalmarson, and C. B. Norris, J. Lumin. **31&32**, 436 (1984).
[48]K. Cho, S. Suga, W. Dreybrodt, and F. Willmann, Phys. Rev. B **11**, 1512 (1975).
[49]H. Venghaus, P. E. Simmonds, P. J. Dean, J. Lagois, and D. Bimberg, Solid State Commun. **24**, 5 (1977).
[50]P. J. Dean, H. Venghaus, J. C. Pfister, B. Schaub, and J. Marine, J. Lumin. **16**, 363 (1978).